

Stable Operation and Current Sharing Control among Parallel Single-Phase Inverter Modules with Unequal Filter Impedances

P. Sarvghai, M. Monfared*

Department of Electrical Engineering, Faculty of Engineering, Ferdowsi University of Mashhad, Mashhad, Iran

Abstract- Parallel connection of two or even more single-phase inverter modules is a successful solution to increase the reliability and the efficiency of an inverter at moderate power levels. Stable operation and proper current sharing among parallel inverter modules is a key issue, especially when they are connected to a common load through unequal output filter impedances. In this paper, a new formulation and consequently a proper current sharing control algorithm for parallel connected inverter modules with the possibility of unequal filter impedances is proposed. Also a dual-loop voltage control with the filter current as the inner loop feedback signal, considering the effect of digital control delay, is adopted. The controller parameters are designed according to a frequency domain analysis. Finally, theoretical achievements are confirmed by experimental test results on a test rig with two 250 W parallel connected single phase inverters.

Keyword: Parallel inverter modules, Circulating current, Load sharing

NOMENCLATURE

N	Number of PIMs
I_o	Output current of PIM
I_{avg}	Average current of each PIM
I_{cc}	Circulating current
I_{CCR}	Real component of circulating current
I_{CCI}	Imaginary component of circulating current
I_f	Filter current
I_c	Capacitor current
u_o	PCC voltage
u	Open circuit voltage of each PIM
R_f	Filter resistance
L_f	Filter inductance
Z_f	Filter impedance
w	Angular frequency
δ	Power angle
$H(s)$	Transfer function of all pass filter
K_{pr}	Proportional coefficient
K_{ir}	Integral coefficient
w_c	Angular cut off frequency
F_{sw}	Switching frequency
T_s	Sampling period

1. INTRODUCTION

Nowadays, parallel inverter modules are more employed to convert energy from renewable systems such as photovoltaics and wind turbines to the local loads or the

distribution grid. Also, they can be used to provide reliable and high quality electric power for sensitive or critical consumers, such as hospitals, military centers, administration offices and so on.

Parallel arrangement of inverters is an industrial solution to increase the power rating and the generated waveform quality. Also, the achieved redundancy provides higher reliability and greater flexibility for further expansions using the available inverter modules. Cost reduction is another practical advantage, because the fractional power inverter modules do not require expensive semiconductor devices with high ratings. Also, it is shown that the parallel inverters offer more efficiency than a central inverter at the same power level [1-3]. Despite these benefits, a technical issue, called circulating current (CC), challenges the performance of the parallel configured inverters, seriously. The CC produces unexpected losses, causes flow of useless power between the parallel inverters and increases the current distortion [4]. A relatively large CC may even lead to instability of the system [5-6]. The CC originates from the possible amplitude deviation or phase shift of the output voltages of the parallel inverter modules (PIMs) compared with the common reference voltage for all modules, due to several practical issues, the main being differences between semiconductor devices and filter parameters.

Various control techniques are already proposed to limit the magnitude of the CC, which can be broadly

Received: 21 Jul. 2021

Revised: 01 Oct. 2021

Accepted: 13 Oct. 2021

*Corresponding author:

E-mail: m.monfared@um.ac.ir (M.Monfared)

DOI: 10.22098/joape.2022.9668.1673

Research Paper

© 2022 University of Mohaghegh Ardabili. All rights reserved.

divided into two main categories: power droop control and active load sharing techniques [7–12]. The aim of droop control techniques is load sharing among parallel inverters through control of voltage and frequency, while no intercommunication among the inverters is required. Conventional droop control [13-14], VPD/FQB droop control [15], voltage-based droop control [16], virtual-structure-based method [17-19] are main solutions proposed in literature. As an important drawback for these methods is the deviation of the voltage and the frequency which is another origin of CC among PIMs [20]. The active load sharing techniques take benefit of information exchange among centrally installed PIMs. The active load sharing techniques use the equivalent Thevenin model of the PIMs to instantaneously regulate the equivalent Thevenin voltage sources such that the measured CC is kept very small. To do that, the reference voltage signal or the output of the voltage regulator of each PIM is continuously modified by the active load sharing algorithm based on the measured currents and the equivalent output impedance of each PIM. Several active load sharing control techniques, such as the centralized, master-slave, distributed and circular chain control are already suggested. In the centralized control the current sharing unit measures the total load current and based on the number of available PIMs, it determines the reference current for each PIM [21-26]. The voltage synchronization among different PIMs is based on a command signal generated by the central unit for individual PIMs. In the master-slave control, the master unit regulates the output voltage and the slave PIMs track the reference current that is produced by the master unit [1, 27-30]. Contrary to the centralized and the master-slave techniques, active load sharing based on the distributed control is not dependent on a central controller or a master PIM and when a defect occurs in any of the PIMs, other modules continue operating at normal condition and only the defected one will be deactivated [22, 31–35]. Aforementioned techniques need a reliable and high bandwidth communication among all PIMs. In order to reduce the interconnections between different PIMs, the circular chain control is recently proposed [36–38]. In this method each PIM receives the reference current command from the previous one. A common weakness among all previous works on the active load sharing techniques is that the effects of mismatches or uncertainties on the output filter parameters are not discussed. While these mismatches, which are unavoidable in practice due to component tolerances and parameter variations (usually arisen from thermal effects and aging), can affect the

performance of the current sharing control and increase the CC.

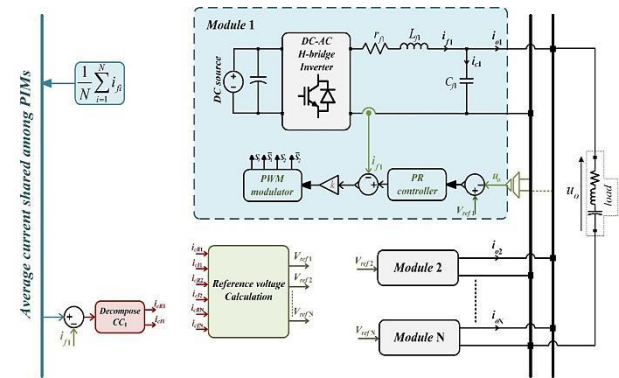


Fig. 1. Simplified model of N single-phase PIMs along with the proposed control system

In the previous works, it is assumed that all of the parallel inverter modules have the same topology and circuit configuration. This is not always possible in practical applications and so there may appear a circulating current among PIMs. One main source of difference among PIMs is unequal filter impedance characteristics. In this paper, a new formulation for the parallel connected inverter modules through LC filters that feed a common local load is developed, which considers the filter parameter differences among the modules. Consequently, a reference voltage calculation algorithm for the PIMs is proposed that ensures stable operation and perfect current sharing control among them under unequal filter impedances. The proposed algorithm does not require either a PLL or a synchronization signal among the PIMs. A dual-loop voltage control scheme with the filter current as the inner loop feedback signal is then adopted. A frequency domain design procedure of the controller parameters, considering the effect of digital implementation delays, is suggested, which offers excellent steady-state and transient performance. Theoretical achievements are finally confirmed through experimental tests under various operating conditions.

In section 2, configuration of the PIMs is investigated. The proposed current sharing control for reduction of CC is then explained in section 3. Design of the close loop feedback control with outer and inner loops is described in section 4. Section 5 presents simulation and experimental results to show the proper performance of the control method. Finally, section 6 concludes the paper.

2. MODELING OF PIMs

The simplified model of N single-phase PIMs along with the proposed control system is shown in Fig. 1. The output of each PIM is connected to the common

load at point of common coupling (PCC) through a LC filter. The PIMs are supplied from isolated DC voltage sources. Any combination of resistive, inductive, capacitive, linear or nonlinear loads can be connected to the PCC. According to Fig. 1, the average current of each PIM can be calculated as:

$$I_{avg} = \frac{1}{N} \sum_{i=1}^N I_{oi} \quad (1)$$

The current I_{avg} is the equal current share of each PIM and if all PIMs achieve this current, one can say that the proper load sharing among all PIMs is occurred. The CC for each PIM can then be readily calculated as:

$$I_{cej} = I_{avg} - I_{oj} \quad (2)$$

It should be noted that in practical applications the filter inductor current, if, is usually measured for both control and overcurrent protection purposes and using an extra current sensor for measuring the PIM output current, i_o , increases the complexity and cost. For this reason and based on Fig. 1, the filter inductor current of each PIM can be calculated as

$$I_{fj} = I_{oj} + I_{Cj} \quad (3)$$

By replacing Eqns. (1) and (3) in Eq. (2), the CC is calculated as

$$I_{cej} = \frac{1}{N} \sum_{i=1}^N I_{fi} - \frac{1}{N} \sum_{i=1}^N I_{Ci} - I_{fj} + I_{Cj} \quad (4)$$

Due to the fact that the instantaneous capacitor voltages of all PIMs are the same and at the same power level, the filter capacitances of all PIMs are also equal, then it can be readily concluded that the capacitor currents are equal and it can be assumed that

$$I_{Cj} = \frac{1}{N} \sum_{i=1}^N I_{Ci} \quad (5)$$

and consequently, Eq. (4) simplifies to

$$I_{cej} = \frac{1}{N} \sum_{i=1}^N I_{fi} - I_{fj} \quad (6)$$

As a result, the CC is calculated from measured filter currents of PIMs. Now, the CC calculated from Eq. (6) is decomposed to real and imaginary components, as shown in Fig. 1, and these components are used by the proposed control strategy, explained in the next section, to generate the reference voltages for all PIMs. Finally, a double-loop regulator for each PIM, including an outer proportional-resonant (PR) voltage controller and an inner simple proportional current controller tracks the reference voltage signal with superior steady-state and transient performance.

3. PROPOSED CURRENT SHARING SCHEME

On the basis described in the previous section, the main

part of the control system of Fig. 1 is the reference voltage generator for the PIMs. In this section, the conditions to ensure proper current sharing among PIMs are first investigated. Theoretically, the same amplitude, phase and frequency of the output voltages are prerequisite to allow connect two or more PIMs in parallel. Any deviation of the mentioned terms can lead to CC flow between the PIMs. For the sake of simplicity, the following study deals with the two single phase PIMs connected in parallel, for which the equivalent circuit is shown in Fig. 2. Due to the inductive-resistive nature of the output filter impedance, the instantaneous voltage equations for the PIMs can be expressed as:

$$\begin{cases} u_1 = u_o + \left(r_{f1} i_{f1} + L_{f1} \frac{di_{f1}}{dt} \right) \\ u_2 = u_o + \left(r_{f2} i_{f2} + L_{f2} \frac{di_{f2}}{dt} \right) \end{cases} \quad (7)$$

Considering that the PCC voltage is the same for both PIMs, then it can be concluded that

$$u_1 - \left(r_{f1} i_{f1} + L_{f1} \frac{di_{f1}}{dt} \right) = u_2 - \left(r_{f2} i_{f2} + L_{f2} \frac{di_{f2}}{dt} \right) \quad (8)$$

In view of Eq. (8), as long as the filter impedances and the instantaneous voltages of PIMs are equal, a perfect current sharing is ensured. However, in practical applications, due to differences of these equivalent impedances, the flow of CC is possible. Nonlinearity of magnetic cores, unequal number of wiring turns, different characteristics of semiconductor devices and finally the thermal effect and aging lead to unequal or even uncertain equivalent output filter impedances. Under this condition, if the system controller and the modulator make the instantaneous output voltages (u_1 , u_2) equal, then the CC flows between PIMs. This current can lead to instability of systems and amplitude of its current should be limited. According to Eq. (6), for the case of two PIMs, the CC in the phasor state can be described as:

$$I_{cc} = \frac{I_{f1} - I_{f2}}{2} \quad (9)$$

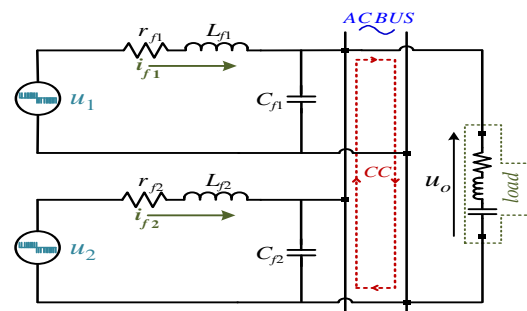


Fig.2. equivalent circuit for PIM

Filter current for each PIM can be calculated from Eq. (7), as

$$\begin{cases} I_{f1} = \frac{U_1 \angle \delta_1 - U_o \angle 0}{Z_{f1}} \\ I_{f2} = \frac{U_2 \angle \delta_2 - U_o \angle 0}{Z_{f2}} \end{cases} \quad (10)$$

Replacing from Eq. (10) in Eq. (9), the CC can be written as Eq. (11).

$$I_{cc} = \frac{1}{2} \left(\frac{U_1 \angle \delta_1 - U_o}{Z_{f1}} - \frac{U_2 \angle \delta_2 - U_o}{Z_{f2}} \right) \quad (11)$$

The CC can be decomposed to the real (I_{cR}) and the imaginary (I_{cI}) components. Considering a small value for $\delta_{1,2}$, then it is reasonable to assume:

$$\begin{cases} \cos \delta_1 = \cos \delta_2 = 1 \\ \sin \delta_1 = \sin \delta_2 = 0 \end{cases} \quad (12)$$

By replacing Eq. (12) into Eq. (11), the real and imaginary components of CC are calculated as

$$I_{ccR} = A_1 U_1 - B_1 U_2 + C_1 U_o \quad (13)$$

$$I_{ccI} = A_2 U_1 - B_2 U_2 + C_2 U_o \quad (14)$$

In above equations, A_1 , A_2 , B_1 , B_2 , C_1 and C_2 are calculated from the equivalent output impedances and are given in the appendix. To achieve the best current sharing among PIMs, the filter currents of all inverters must be the same, i.e.:

$$I_f = I_{f1} = I_{f2}. \quad (15)$$

As a result, given that the output impedances of different inverters are not equal, then it can be concluded that:

$$\begin{cases} U_o = U_1 - Z_{f1} I_f \\ U_o = U_2 - Z_{f2} I_f \end{cases} \quad (16)$$

Where

$$\begin{cases} Z_{f1} = r_{f1} + jL_{f1}\omega \\ Z_{f2} = r_{f2} + jL_{f2}\omega \end{cases} \quad (17)$$

At parallel condition, the PCC voltage is the same for all PIMs, consequently Eqns. (16) and (17) indicate that the inverter with the larger output filter impedance should have a larger open circuit voltage (U_1 , U_2). By simultaneous solving of Eqns. (13) and (14), with the measured U_o and I_{cc} and known filter parameters, the open circuit voltage of each PIM is determined. The detailed block diagram of the reference voltage generator is shown in Fig. 3. As a result, stable operation with the same PCC voltage, proper current sharing among the PIMs and suppression of the CC are ensured.

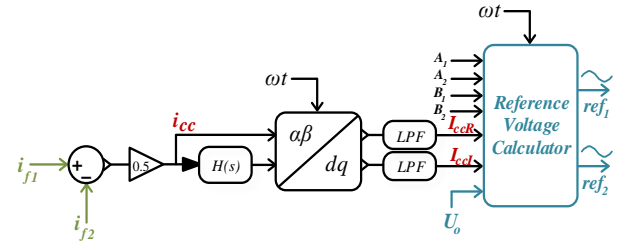


Fig. 3. Block diagram of reference voltage calculation.

As can be seen in Fig. 3, in order to compute the real and imaginary components of the CC, first a fictitious second phase current ($i_{c\beta}$) is generated from the original current signal ($i_{c\alpha}$) as:

$$i_{c\alpha} = i_c \quad (18)$$

$$i_{c\beta} = H(s)i_c \quad (19)$$

$$H(s) = \frac{-s + \omega}{s + \omega} \quad (20)$$

Then it is possible to transform the CC to the synchronous reference frame, as expressed by Eq. (21) [29].

$$\begin{pmatrix} i_{cd} \\ i_{cq} \end{pmatrix} = \begin{pmatrix} \cos \omega t & \sin \omega t \\ -\sin \omega t & \cos \omega t \end{pmatrix} \begin{pmatrix} i_{c\alpha} \\ i_{c\beta} \end{pmatrix} \quad (21)$$

First order low pass filters (LPFs) with the cut-off frequency of about 50 Hz are used to attenuate the harmonic components of the real and imaginary components.

4. DESIGN OF FEEDBACK CONTROL

In order to ensure proper performance at transient and steady-state conditions and successful current sharing a double loop control scheme, consisting of an outer voltage control and an inner current control are adopted here. Hence the quality of the output voltage cannot be compromised in an UPS application, then a high performance proportional-resonant (PR) controller is used as the outer voltage controller, which ensures zero-tracking error of sinusoidal signals. The PR controller transfer function is shown in Eq. (22) where K_{pr} and K_{ir} are the proportional and the resonator gains, respectively and ω_c is the bandwidth centered at the resonance frequency ω [39-40].

$$G_{PR}(s) = K_{pr} + \frac{K_{ir}s}{s^2 + 2\omega_c s + \omega^2} \quad (22)$$

Although it is possible to use a proportional-integral (PI) instead, but it should be noted that the PI has its high gain at the zero frequency and therefore a zero steady-state error with the sinusoidal reference cannot be achieved. As a result a CC may flow among PIMs. The inner current controller is a simple proportional controller, K_{pi} , which has a simple structure and offers a

fast dynamic response with no phase-shift of the AC signal. The block diagram of the double-loop voltage control is shown in Fig. 4 where

$$G_L(s) = \frac{1}{sL_f + r_f} \quad (23)$$

$$G_c(s) = \frac{1}{sC_f} \quad (24)$$

And the loop gain can be readily written as

$$G_{open-loop}(s) = \left(K_{pr} + \frac{K_{ir}s}{s^2 + 2\omega_c s + \omega^2} \right) \left(\frac{K_{pi} H_{delay} G_L G_c}{1 + K_{pi} H_{delay} G_L G_c} \right) \quad (25)$$

Where H_{delay} , as expressed by Eq. (26), represents the total delay of digital control system that highly affects the design of controller parameters and analysis of system performance. The existence of delay in a digital control system decreases the phase margin and can even lead to instability.

$$H_{delay}(s) = e^{-s\sigma T_s} \quad (26)$$

In Eq. (26), T_s is the digital sampling period, which is usually equal to the switching period and σ is a constant value between 1 and 2. A simple linear approximation of Eq. (26) is

$$H_{delay}(s) = \frac{1 - s\sigma \frac{T_s}{4}}{1 + s\sigma \frac{T_s}{4}} \quad (27)$$

Then, the loop gain transfer function can be rewritten as Eq. (28) where $\sigma = 1.5$ and $\omega_c = 0.1$ rad/s.

$$G_{open-loop}(s) = \frac{(K_{pr}s^2 + (K_{ir} + 2K_{pr}\omega_c)s + K_{pr}\omega^2)}{(s^2 + 2\omega_c s + \omega^2)} \cdot \frac{-K_{pi}((3\sigma T_s)s/8 - 1)(K_{pr} + (K_{ir}s)/(s^2 + 2\omega_c s + \omega^2))}{(sC((3\sigma T_s)s/8 + 1)(r + Ls)(1/(sC(r + Ls)))} \quad (28)$$

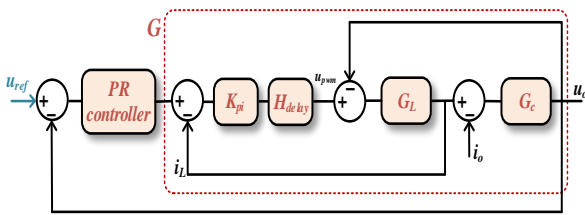


Fig.4. Block diagram of control system

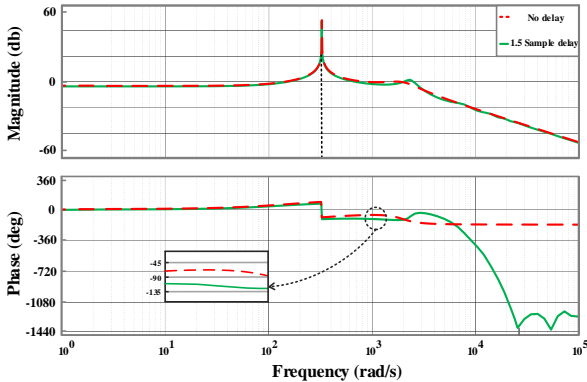


Fig.5. Bode open loop plot of voltage control scheme

To ensure a fast dynamic response while prevent the switching noises from affecting the control system, one can choose the gain cross-over frequency about one-fifth of the switching frequency [41], [42]. Therefore, K_{pr} can be calculated from

$$\begin{cases} |G_{open-loop}(j2\pi f_g)| = 1 \\ f_g \cong 0.2 f_{sw} \end{cases} \quad (29)$$

as $K_{pr} = 0.2$ where f_g and $f_{sw} = 5$ kHz are the cross-over and switching frequencies, respectively.

In above calculations it is assumed that the resonator gain has no effect on the dynamic performance of the control system. In order to eliminate the steady state error, K_{ir} is then chosen large enough, however a very large K_{ir} may decrease the phase margin and cause oscillatory response or even instability. Based on this assumption, K_{ir} is chosen 550, which translates to a system phase margin of about 60 (deg) at the cross-over frequency of 942 Hz that is quite enough in most power electronic applications. The Bode plot of open loop system is shown in Fig. 5.

5. PERFORMANCE EVALUATION

To confirm the feasibility of the proposed control algorithm, simulation is done with Simulink/MATLAB. Simulation accomplished in steady-state with two states as, linear and non-linear loads. In Fig. 6, the output voltage and the current sharing among PIMs and the CC are depicted. Based on this figure, the THD (total harmonic distortion) of the output voltage is around 0.4% and $i_1=7.1$ A and $i_2=7.08$ A.

Percentage of the CC with respect to the total load current is about 0.7%. Current sharing control with nonlinear load is also very good and the THD of the output voltage under this state is around 5.8%. The waveforms with the nonlinear load are shown in Fig. 7. In this case the CC equals to 200mA, which translates to around 1.1%. To confirm the proper operation of the proposed PIMs control algorithm an experimental setup, shown in Fig.8, is prepared in the laboratory. This setup consists of two 500 W inverters connected in parallel via LC filters. The load sharing algorithm and the double-loop voltage controllers are implemented on a 150 MHz digital signal controller (DSC) TMS320F28335 from Texas Instruments. The parameters of the setup are listed in Table 1.

5.1. Load sharing among PIMs

The proper current sharing among PIMs under linear and nonlinear loading is confirmed here. In the first study, three scenarios based on the filter impedance

changes and with a resistive load are examined. In all scenarios, listed in Table 2, the filter impedance of inverter 1 is kept unchanged while the filter impedance of the second inverter changes accordingly. Experimental results for three scenarios are shown in Fig. 9. In this figure the PCC voltage and the output currents of two inverters, as well as the circulating current calculated with the math function of the TEK oscilloscope are presented. Apparently, in the worst-case condition the CC to the nominal current is about 1.1 percent. This means that the proposed algorithm offers an excellent performance and ensures stable operation under large impedance differences. Moreover, the total harmonic distortion (THD) of the output voltage, measured by a Fluke 435, is 0.6%. In the two next studies, first a resistive-inductive then a diode rectifier feeding a resistive-capacitive load, as a highly nonlinear load, are connected to the output of PIMs. Again, as a worst case of filter impedance differences, case 3 of Table 2 is implemented.

Table 1. Parameters of pims

Parameters	Symbol	Value
DC link voltage	V_{DC}	55V
AC bus voltage	V_{AC}	45 V MAX
Filter capacitance	C_f	32 μ F
Filter inductance and equivalent resistance	L_f, r_f	Table 2
Load resistance	R_o	2.2 Ω
Load inductance	L_o	4 mH
Switching frequency	f_s	5 KHz

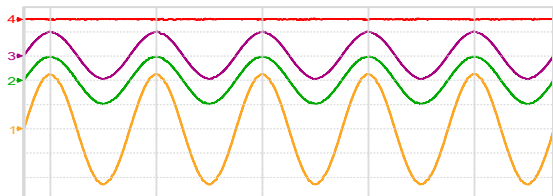


Fig.6. Simulation of proposed control at linear case 1: 20 V/div 2: 10 A/div 3: 10 A/div 4: 10 A/div time scale 10 ms/div

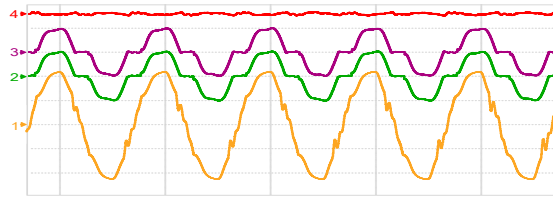


Fig.7. Simulation of proposed control at non-linear case 1: 20 V/div 2: 10 A/div 3: 10 A/div 4: 10 A/div time scale 10 ms/div

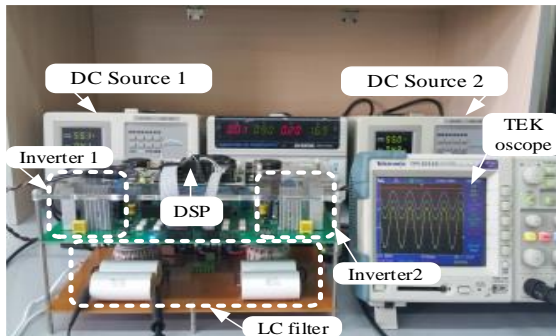


Fig.8. Experimental setup

Table 2. Scenarios of filter impedance differences

Case	Filter impedance 1	Filter impedance 2
1	$(31+j0.82\omega)$ m Ω	$(19+j0.61\omega)$ m Ω
2	$(31+j0.82\omega)$ m Ω	$(29+j0.805\omega)$ m Ω
3	$(31+j0.82\omega)$ m Ω	$(43+j1.1\omega)$ m Ω

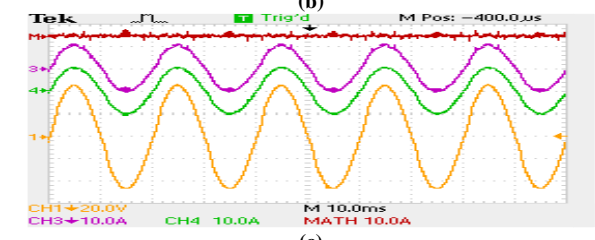
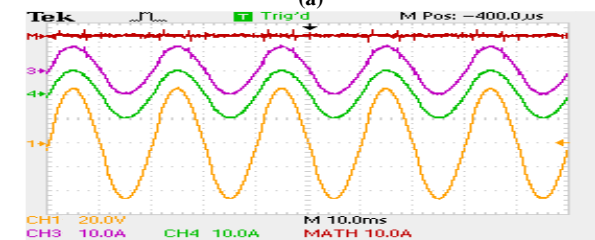
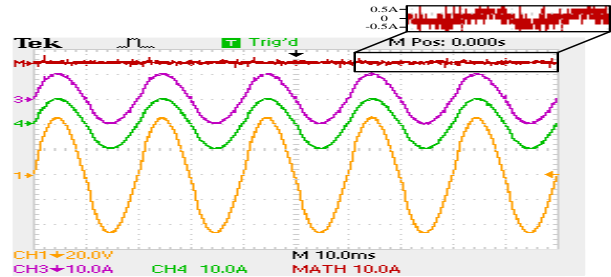


Fig.9. Load sharing performance under large filter impedance differences with resistive load (a) case 1, (b) case 2 and (c) case 3; CH 1: PCC voltage (20V/div); CH 3, 4: output currents (10A/div); M: circulating current (10A/div)

Figs. 10 and 11 show the perfect current sharing performance under these conditions. The THDs of PCC voltages are 1.9% and 6.2% for Figs. 10 and 11, respectively. The results of load sharing studies with linear and nonlinear loads are summarized in Table 3 where the CC is kept negligible under all test conditions.

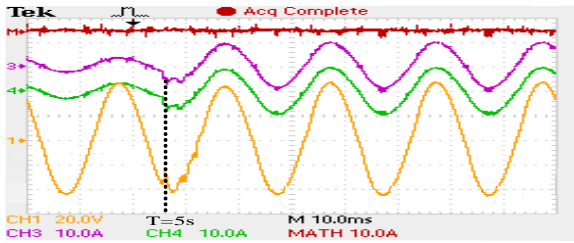
5.2. Double loop controller performance

Because the connected load at output of UPS is not fixed and may experience severe changes, the proper operation at transient states is critical. This goal is achieved with proper design of controllers' parameters for a fast dynamic response. In the following, the transient performance of double-loop feedback control in response to step changes of load and reference voltage is studied and the results are shown in Figs.11 and 12, respectively. As the worst cases all step changes occurred at the voltage/current peaks. In all conditions, a fast and smooth transient performance is obvious. The voltage waveform recovers in less than some milliseconds without experiencing any considerable

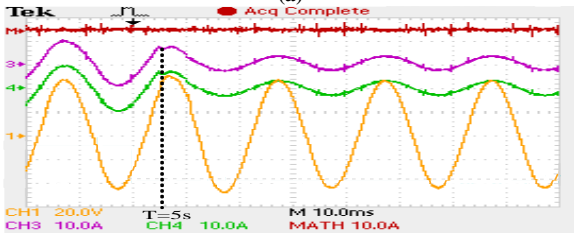
oscillation. Also the current sharing performance is not affected during the transient time, which means a robust operation against the load and reference changes.

5.3. Comparison Study

A current decoupling parallel control strategy of single-phase inverter is presented in Ref. [43]. In that paper voltage reference calculated by using the active and reactive parts of the circulating current. That paper considers only the imaginary part of the filter impedance in calculating the reference voltage. Moreover, the reference voltage of each inverter is the same, which with little mismatch in filter impedance characteristics a circulating current flows between the parallel inverters. In the proposed method, both real and imaginary parts of the impedance are considered. In addition, the reference voltage is calculated separately for each inverter.

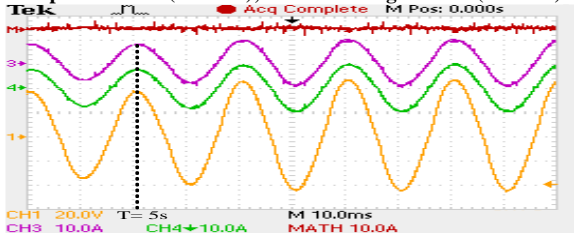


(a)

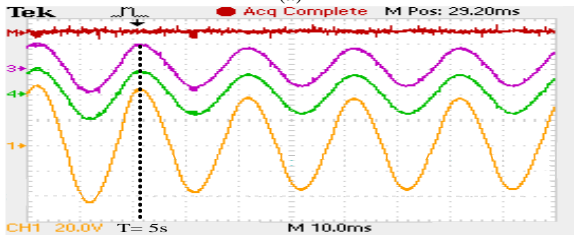


(b)

Fig.11. Transient performance in response to (a) step-up and (b) step-down load changes; CH 1: PCC voltage (20V/div); CH 3, 4: output currents (10A/div); M: circulating current (10A/div)



(a)



(b)

Fig.12. Transient performance in response to (a) step-up and (b) step-down reference voltage changes; CH 1: PCC voltage (20V/div); CH 3, 4: output currents (10A/div); M: circulating current (10A/div)

Table 3. Peak to Peak Circulating Current

	Linear	Resistive-Inductive	Non-Linear
Conventional control[43]	2.4 A	2.4 A	8 A
Proposed Control	1 A	1.5 A	2 A

In the proposed control strategy any changes in the filter impedance directly affect the calculated reference voltage. As a result, proper load sharing among PIMs is guaranteed by this control method. Moreover, feedback control of this paper is proportional-resonant, which in comparison to the PI controller of Ref. [43] has a faster response and ensures zero-tracking error of sinusoidal signals. This controller along with the proposed control strategy helps proper current sharing among PIMs. Comparison between the proposed current sharing and the conventional control method [43] is done and the peak to peak circulating current results are listed as Table 3.

Based on Table 2, the third case scenario is considered where the mismatch between filter impedance of each inverter is remarkable. Simulation accomplished in the steady-state with three different loading as, linear, resistive-inductive and non-linear loads. From the results it is clear that the amplitude of the circulating current is much smaller in the proposed technique than the conventional one that is more evident under non-linear load.

6. CONCLUSION

In this paper, a current sharing control method was proposed and evaluated experimentally on a system of two 500W PIMs under three different scenarios, such as linear inductive and non-linear loads. Based on the experimental results, circulating current in all studies is very low and the proposed method presents excellent steady-state and transient performance. Besides, the proportional-resonant voltage controller, tuned in the frequency domain, makes it possible to track the reference voltages already generated by the proposed current sharing algorithm fast and smoothly.

Appendix A.

The parameters A_1 , A_2 , B_1 , B_2 , C_1 and C_2 of equations (13) and (14) are:

$$\begin{cases} X_{f1} = jL_{f1}\omega \\ X_{f2} = jL_{f2}\omega \end{cases} \quad (A.1)$$

$$A_1 = \frac{8(R_1R_2^2 + R_1X_{f2}^2)}{(4R_1R_2 - 4X_{f1}X_{f2})^2 + (4R_1X_{f2} + 4X_{f1}R_2)^2} \quad (A.2)$$

$$A_2 = \frac{-8(X_{f1}X_{f2}^2 + X_{f1}R_2^2)}{(4R_1R_2 - 4X_{f1}X_{f2})^2 + (4R_1X_{f2} + 4X_{f1}R_2)^2} \quad (A.3)$$

$$B_1 = \frac{8(R_1^2 R_2 + X_{f1}^2 R_2)}{(4R_1 R_2 - 4X_{1f} X_{f2})^2 + (4R_1 X_{f2} + 4X_{f1} R_2)^2} \quad (\text{A.4})$$

$$B_2 = \frac{8(X_{f1}^2 X_{f2} + R_1^2 X_{f2})}{(4R_1 R_2 - 4X_{1f} X_{f2})^2 + (4R_1 X_{f2} + 4X_{f1} R_2)^2} \quad (\text{A.5})$$

$$C_1 = \frac{8(R_1^2 R_2 - R_1 R_2^2 - R_1 X_{f2}^2 + X_{f1}^2 R_2)}{(4R_1 R_2 - 4X_{1f} X_{f2})^2 + (4R_1 X_{f2} + 4X_{f1} R_2)^2} \quad (\text{A.6})$$

$$C_2 = \frac{8(X_{f1} X_{f2}^2 - X_{f1}^2 X_{f2} - R_1^2 X_{f2} + X_{f1} R_2^2)}{(4R_1 R_2 - 4X_{1f} X_{f2})^2 + (4R_1 X_{f2} + 4X_{f1} R_2)^2} \quad (\text{A.7})$$

REFERENCES

- [1] J. Chen and C. Chu, "Combining droop and direct current vector control for control of parallel inverters in microgrid", *IET Renew. Power Gener.*, vol. 11, pp. 107-114, 2017.
- [2] S. Kazemi, M. Parniani and M. Rasouli, "The effects of excitation control systems on parallel operation of DGs with the main grid", *J. Iran. Assoc. Electr. Electron. Eng.*, vol. 4, 2007.
- [3] A. Abdollahi, S. Nikraves and M. Menhaj, "An intelligent control strategy in a parallel hybrid vehicle", *J. Iran. Assoc. Electr. Electron. Eng.*, vol. 4, 2007.
- [4] I. Lorzadeh et al., "Hierarchical control for accurate sharing of reactive power and harmonic currents in islanded microgrids based on instantaneous circulating currents", *J. Iran. Assoc. Electr. Electron. Eng.*, vol. 13, pp. 57-72, 2016.
- [5] M. Zhang et al., "Control strategy design and parameter selection for suppressing circulating current among SSTs in parallel", *IEEE Trans. Smart Grid*, vol. 6, pp. 1602-09, 2015.
- [6] P. Sarvghadi and M. Monfared, "Load sharing control of parallel inverters with uncertainty in the output filter impedances for islanding operation of AC micro-grid", *22nd Electr. Power Distrib. Conf.*, 2017.
- [7] C. Song et al., "Circulating current elimination scheme for parallel operation of common DC bus inverters", *Int. J. Electr. Power Energy Syst.*, vol. 63, pp. 17-29, 2014.
- [8] W. Yao et al., "Design and analysis of the droop control method for parallel inverters considering the impact of the complex impedance on the power sharing", *IEEE Trans. Ind. Electron.*, vol. 58, pp. 576-588, 2011.
- [9] W. Chen et al., "A fully modular control strategy for input-series output-parallel (ISOP) inverter system based on positive output-voltage-amplitude gradient", *IEEE Trans. Power Electron.*, vol. 33, pp. 2878-87, 2018.
- [10] J. Guerrero et al., "Control strategy for flexible microgrid based on parallel line-interactive UPS systems", *IEEE Trans. Ind. Electron.*, vol. 56, pp. 726-36, 2009.
- [11] Z. Chen et al., "An adaptive virtual resistor (AVR) control strategy for low-voltage parallel inverters", *IEEE Trans. Power Electron.*, vol. 8993, pp. 863-76, 2018.
- [12] X. Sun et al., "Design and analysis of an optimal controller for parallel multi-inverter systems", *IEEE Trans. Circuits Syst.*, vol. 52, pp. 56-61, 2006.
- [13] F. Katiraei and M. Iravani, "Power management strategies for a microgrid with multiple distributed generation units", *IEEE Trans. Power Syst.*, vol. 21, pp. 1821-31, 2006.
- [14] E. Coelho, P. Cortizo, and P. Garcia, "Small-signal stability for parallel-connected inverters in stand-alone ac supply systems", *IEEE Trans. Ind. Appl.*, vol. 38, pp. 533-42, 2002.
- [15] C. Sao and P. Lehn, "Control and power management of converter fed microgrids", *IEEE Trans. Power Syst.*, vol. 23, pp. 1088-98, 2008.
- [16] T. Vandoorn et al., "A control strategy for islanded microgrids with DC-link voltage control", *IEEE Trans. Power Deliv.*, vol. 26, pp. 703-13, 2011.
- [17] J. Guerrero et al., "Advanced control architectures for intelligent microgrids; part I: decentralized and hierarchical control", *IEEE Trans. Ind. Electron.*, vol. 60, pp. 1254-62, 2013.
- [18] J. Guerrero, J. Vasquez and R. Teodorescu, "Hierarchical control of droop-controlled DC and AC microgrids-a general approach towards standardization", *35th Annual Conf. IEEE Ind. Electron.*, vol. 58, pp. 4305-10, 2009.
- [19] J. He et al., "An islanding Microgrid power sharing approach using enhanced virtual impedance control scheme", *IEEE Trans. Power Electron.*, vol. 28, pp. 5272-82, 2013.
- [20] J. He and Y. Li, "An enhanced microgrid load demand sharing strategy", *IEEE Trans. Power Electron.*, vol. 27, pp. 3984-95, 2012.
- [21] M. Hamzeh, S. Farhangi, and M. Sanayepasand, "A new method for analysis of frequency based anti-islanding protection in multiple inverters situation", *J. Iran. Assoc. Electr. Electron. Eng.*, vol. 9, pp. 11-18, 2012.
- [22] M. Ramezani, S. Li, and Y. Sun, "Combining droop and direct current vector control for control of parallel inverters in microgrid", *IET Renew. Power Gener.*, vol. 11, pp. 107-14, 2017.
- [23] K. Siri, "Current distribution control for parallel connected converters: part I", *IEEE Trans. Aerosp. Electron. Syst.*, vol. 28, pp. 829-40, 1992.
- [24] T. Wu, K. Siri, and J. Banda, "The central-limit control and impact of cable resistance in current distribution for parallel-connected DC-DC converters", *Proc. 1994 Power Electron. Spec. Conf.*, 1994.
- [25] J. Banda and K. Siri, "Improved central-limit control for parallel-operation of DC-DC power converters", *Proc. 1995 - Power Electron. Spec. Conf.*, 1995.
- [26] M. Abdelaziz et al., "A multistage centralized control scheme for islanded microgrids with PEVs", *IEEE Trans. Sustain. Energy*, vol. 5, pp. 927-37, 2014.
- [27] T. Caldognetto and P. Tenti, "Microgrids operation based on master-slave cooperative control", *IEEE J. Emerg. Sel. Top. Power Electron.*, vol. 2, pp. 1081-8, 2014.
- [28] Y. Pei et al., "Auto-master-slave control technique of parallel inverters in distributed AC power systems and UPS", *IEEE 35th Annual Power Electron. Spec. Conf.*, vol. 3, pp. 2050-3, 2004.
- [29] F. Petruzzello, P. Ziogas, and G. Joos, "A novel approach to paralleling of power converter units with true redundancy", *21st Annual IEEE Conf. Power Electron. Spec.*, 1990.
- [30] A. Zorig et al., "Novel differential current control strategy based on a modified three-level SVPWM for two parallel-connected inverters", *IEEE J. Emerg. Sel. Top. Power Electron.*, vol. 5, pp. 1807-18, 2017.
- [31] H. Xin et al., "Control of island AC microgrids using a fully distributed approach", *IEEE Trans. Smart Grid*, vol. 6, pp. 943-45, 2015.
- [32] X. Jiang et al., "A novel wireless control strategy for input-series output-parallel inverter system", *IEEE Energy Conv. Congr. Expos.*, vol. 2, pp. 2156-60, 2017.

- [33] A. Ketabi, S. Rajamand, and M. Shahidehpour, "Power sharing in parallel inverters with different types of loads", *IET Gener. Transm. Distrib.*, vol. 11, pp. 2438-47, 2017.
- [34] Q. Shafiee, J. Vasquez, and J. Guerrero, "Distributed secondary control for islanded MicroGrids - A networked control systems approach", *IECON Proc. Ind. Electron. Conf.*, pp. 5637-42, 2012.
- [35] A. Bidram, A. Davoudi, and F. Lewis, "A multiobjective distributed control framework for islanded AC microgrids", *IEEE Trans. Ind. Inf.*, vol. 10, pp. 1785-98, 2014.
- [36] W. Tsai-Fu and Y. Chen, "3C strategy for inverters in parallel operation achieving an equal current distribution", *IEEE Trans. Ind. Electron.*, vol. 47, pp. 273-81, 2000.
- [37] P. Electronics, "A 3G strategy for multi-module inverters in parallel operation to achieve an equal current distribution", *Proc. 1998 - Power Electron. Spec. Conf.*, pp. 186-192, 1998.
- [38] K. Piboonwattanakit and W. Khan-ngern, "Design of the two parallel inverter modules by circular chain control technique", *7th Int. Conf. Power Electron. Drive Syst.*, pp. 1518-22, 2007.
- [39] S. Shokoohi et al., "Transient stability enhancement in microgrids including inverter interfaced distributed generation", *J. Iran. Assoc. Electr. Electron. Eng.*, 2015.
- [40] M. Monfared, S. Golestan, and J. Guerrero, "Analysis, design, and experimental verification of a synchronous reference frame voltage control for single-phase inverters", *IEEE Trans. Ind. Electron.*, vol. 61, pp. 258-69, 2014.
- [41] H. Gholami-Khesht, S. Golestan, and M. Monfared, "Low computational burden grid voltage estimation for grid connected voltage source converter-based power applications", *IET Power Electron.*, vol. 8, pp. 656-64, 2015.
- [42] S. Parker, B. McGrath, and D. Holmes, "Regions of active damping control for LCL filters", *IEEE Trans. Ind. Appl.*, vol. 50, pp. 424-32, 2014.
- [43] S. Xu, J. Wang, and J. Xu, "A current decoupling parallel control strategy of single-phase inverter with voltage and current dual closed-loop feedback", *IEEE Trans. Ind. Electron.*, vol. 60, pp. 1306-13, 2011.